Acta Oceanol. Sin., 2023, Vol. 42, No. 2, P. 56–64
https://doi.org/10.1007/s13131-022-2072-7
http://www.aosocean.com
E-mail: ocean2@hyxb.org.cn

Basis functions for shallow-water temperature profiles based on the internal-wave eigenmodes

Qianqian Li[1, 2, 3], Shoulian Cao[1], Yu Luo[1]*, Kai Zhang[1], Fanlin Yang[1]

[1] College of Geodesy and Geomatics, Shandong University of Science and Technology, Qingdao 266590, China

[2] State Key Laboratory of Acoustics, Institute of Acoustics, Chinese Academy of Sciences, Beijing 100190, China

[3] College of Underwater Acoustic Engineering, Harbin Engineering University, Harbin 150001, China

Received 18 February 2022; accepted 1 May 2022

Abstract

The shallow-water temperature profile is typically parameterized using a few empirical orthogonal function (EOF) coefficients. However, when the experimental area is poorly known or highly variable, the adaptability of the EOFs will be significantly reduced. In this study, a new set of basis functions, generated by combining the internal-wave eigenmodes with the average temperature gradient, is developed for characterizing the temperature perturbations. Temperature profiles recorded by a thermistor chain in the South China Sea in 2015 are processed and analyzed. Compared to the EOFs, the new set of basis functions has higher reconstruction accuracy and adaptability; it is also more stable in ocean regions that have internal waves.

Key words: temperature profile, basis function, internal-wave eigenmode, EOF, sound speed profile

Citation: Li Qianqian, Cao Shoulian, Luo Yu, Zhang Kai, Yang Fanlin. 2023. Basis functions for shallow-water temperature profiles based on the internal-wave eigenmodes. Acta Oceanologica Sinica, 42(2): 56–64, doi: 10.1007/s13131-022-2072-7

1 Introduction

The most important acoustic parameter in the ocean is temperature, which is the most basic physical quantity affecting the propagation of sound waves. In an actual ocean environment, temperature exhibits pronounced spatiotemporal variations (Li et al., 2021), and its temporal variability is mainly caused by seasonal changes and the mesoscale phenomena on the ocean (Jensen et al., 2011). The temperature profile can be expressed as a matrix in time or space; however, this requires many parameters, and a certain parsimonious representation technology is necessary for regularizing the temperature profile (Tan et al., 2013). Subsequently, the temperature profile can be approximated using only a few coefficients. The applicability of the parsimonious representation method and whether the basis functions can effectively reflect the physical characteristics of the dynamic marine processes has become a key problem in acoustic monitoring.

To reduce the size of the parameters, the temperature profile is often regularized by the sum of leading order empirical orthogonal functions (EOFs) (Kakatkar et al., 2020). EOFs are derived using principal component analysis (PCA) (Monahan et al., 2009). Many theoretical studies and practical applications have confirmed the effectiveness of EOFs (Li et al., 2015); however, when the number of training samples is too small or does not cover the dynamic ocean cycle, the EOFs often yield low reconstruction accuracy. Li et al. (2019b) used EOFs to build model predictions and indicated that the reason for the prediction having a relatively large error is that the background field changes significantly at long timescales.

The long sample time and wide measurement area necessary for acquiring basis functions are among the main causes that limit the application of EOFs in case of fast ocean changes. Regularizing highly accurate ocean-temperature profiles while using short sampling times is a necessity. Tielbürger et al. (1997) expressed the water-particle displacements associated with the internal-wave field as the sum of a complete orthogonal set of internal-wave eigenmodes with different frequencies. This motivated us to investigate the basis functions for ocean temperature profiles based internal-wave eigenmodes.

The horizontal stratification of shallow seas has both seasonal stability and transient stochastic nature. The stochastic nature of shallow seas is caused by several stochastic components, such as internal waves, tides, and turbulence. Generally, transient disturbances are restricted by a stable background field; therefore, when the stratification characteristics of the background field are known, the transient temperature disturbance at a certain time can be inferred. The background ocean field can be obtained from historical data, such as the Argo network data set or from the average temperature and salinity profiles obtained from small amount of measurement data. In this study, temperature turbulence is reconstructed through numerical experiments in which the sources of randomness are internal waves. The new set of basis functions (termed internal-wave modes; IWMs) is generated by combining the internal-wave eigenmodes with the average temperature gradient. Compared to the EOFs, which require

Foundation item: The Natural Science Foundation of Shandong Province of China under contract Nos ZR2022MA051 and ZR2020MA090; the Fund of China Postdoctoral Science Foundation under contract No. 2020M670891; the Shandong University of Science and Technology Research Fund under contract No. 2019TDJH103; the Talent Introduction Plan for Youth Innovation Team in Universities of Shandong Province (Innovation Team of Satellite Positioning and Navigation).
*Corresponding author, E-mail: luoyu@sdust.edu.cn

extensive and continuous temperature samples, the IWMs can be calculated from the mean background temperature and salinity fields. Meanwhile, the IWMs and their corresponding coefficients are directly related to the dynamic ocean processes; hence, the IWMs have a clearer physical significance than that of the EOFs.

The remainder of this paper is organized as follows: the EOFs and sparse reconstruction methods are described in Section 2; a new set of basis functions is explained in Section 3; the temperature-profile reconstruction results are presented in Section 4; and a summary and conclusions are presented in Section 5.

2 EOFs and compression (Li et al., 2019a)

The EOFs provide a compact representation of the total statistical nature of the temperature data. It is assumed that the temperature matrix is $\boldsymbol{T}$, and is sampled over K discrete points in depth and M instants in time,

$$\boldsymbol{T}=\begin{bmatrix} T_{11} & T_{12} & \cdots & T_{1M} \\ T_{21} & T_{22} & \cdots & T_{2M} \\ \vdots & \vdots & \vdots & \vdots \\ T_{K1} & T_{K2} & \cdots & T_{KM} \end{bmatrix}. \tag{1}$$

After averaging the M temperature profiles, the mean temperature is obtained as $\overline{\boldsymbol{T}}=[\overline{T}_1,\overline{T}_2,\cdots,\overline{T}_K]^{\mathrm{T}}$. Here, $(\cdot)^{\mathrm{T}}$ is a transpose operation. The mean temperature is subtracted to obtain the residual temperature $\boldsymbol{C}$, i.e., $\boldsymbol{C}=\boldsymbol{T}-\overline{\boldsymbol{T}}$.

Matrix $\boldsymbol{A}$ is defined as the covariance matrix of $\boldsymbol{C}$ (i.e., $\boldsymbol{A}=\boldsymbol{C}\boldsymbol{C}^{\mathrm{T}}\in R^{K\times K}$). The singular value decomposition for matrix C is

$$\boldsymbol{C}^{\mathrm{T}}=\boldsymbol{U}\Sigma\boldsymbol{V}^{\mathrm{T}}, \tag{2}$$

where $\boldsymbol{V}=[v_1,\cdots,v_K]\in R^{K\times K}$ are eigenvectors of matrix $\boldsymbol{A}$ and are used as EOFs, and $\boldsymbol{X}=\boldsymbol{U}\Sigma\in R^{M\times K}$are the coefficients. The temperature can be reconstructed by retaining only the leading P-order EOFs,

$$\widehat{\boldsymbol{T}}=\overline{\boldsymbol{T}}+\boldsymbol{V}_P\boldsymbol{X}_P^{\mathrm{T}}, \tag{3}$$

where $\boldsymbol{V}_P\in R^{K\times P}$ is the basis function containing the leading P-order EOFs, and $\boldsymbol{X}_P\in R^{M\times P}$ is the coefficient vector. Usually, for ocean temperatures, $P\leqslant 5$; in this study, we have made P=5.

The EOFs represent the mode of data. Thus, the reconstruction accuracy can be improved by a longer sample time. This is verified by experimental data analysis in Section 4.

3 Orthogonal basis functions based on internal-wave eigenmodes

3.1 *The internal-wave displacement*

It is assumed that the internal-wave displacement field $\eta(r,z,t)$ can be written in the form $\eta(r,z,t)=\eta_{\mathrm{D}}(r,z,t)+\eta_{\mathrm{S}}(r,z,t)$, where η_{D} represents the linear component and η_{S} is the soliton contribution.

The linear displacement can be expressed as the sum of the eigenmodes,

$$\eta_{\mathrm{D}}(r,z,t)=\sum_{k_h}\sum_{j}F(k_h,j)W(k_h,j,z)\mathrm{e}^{\mathrm{i}[k_h r-\omega(k_h,j)t]}, \tag{4}$$

where the weighting factors $F(k_h,j)$ are zero-mean and complex Gaussian random variables with an associated power spectrum. The internal-wave eigenmodes W can be obtained by solving the linearized Navier-Stokes equation for an inviscid, incompressible, and stratified fluid (Tielbürger et al., 1997). k_h is the horizontal wave number, and eigenvalues ω are over a range of $\omega\in[f_c,N_{\max}]$, corresponding to the inertial frequency and the maximum value of the buoyancy frequency.

The second component of the internal-wave field is a soliton displacement field, $\eta_{\mathrm{S}}(r,z,t)$, which represents the nonlinear interaction of oceanic tides with bathymetric features. Limiting the area of interest to the exterior of the source region and considering only the left-propagating waves, η_{S} can be written as

$$\eta_{\mathrm{S}}(r,z,t)=\sum_{k_h}\sum_{j}a_j(r,t)W(k_h,j,z), \tag{5}$$

where a_j is the coefficient.

3.2 *IWMs and compression*

Water temperature satisfies the thermodynamic formulas (Apel, 1987), and internal-wave propagation can be assumed to be an adiabatic process with no heat source. The thermodynamic formula can be simplified as (Song et al., 2014)

$$\frac{\partial T(r,z,t)}{\partial t}+\eta(r,z,t)\times\nabla T(r,z,t)=0. \tag{6}$$

Generally, the horizontal temperature gradient is much smaller than the vertical one, i.e., $\partial T/\partial r$ is much smaller than $\partial T/\partial z$. Therefore, Eq. (6) can be simplified as

$$\frac{\partial T}{\partial t}+\eta\frac{\partial T}{\partial z}=0. \tag{7}$$

Substituting Eq. (4) into Eq. (7), it becomes

$$\frac{\partial T}{\partial t}=-\eta_{\mathrm{D}}\frac{\partial T}{\partial z}=-\frac{\partial T}{\partial z}\sum_{k_h}\sum_{j}F(k_h,j)W(k_h,j,z)\mathrm{e}^{\mathrm{i}[k_h r-\omega(k_h,j)t]}. \tag{8}$$

Let the background temperature is $\overline{T}$ and the disturbance is T', then the temperature profile could be written as $T=\overline{T}+T'$. If $\mathrm{d}\overline{T}/\mathrm{d}z\gg\mathrm{d}T'/\mathrm{d}z$, then $\partial T/\partial z\approx\mathrm{d}\overline{T}/\mathrm{d}z$. Integrating both sides of Eq. (8), it becomes

$$T(z,t)-\overline{T}(z)=\frac{1}{\mathrm{i}\omega}\frac{\mathrm{d}\overline{T}}{\mathrm{d}z}\sum_{k_h}\sum_{j}F(k_h,j)W(k_h,j,z)\mathrm{e}^{\mathrm{i}[k_h r-\omega(k_h,j)t]}. \tag{9}$$

When considering $B_{k_h,j}=\dfrac{F_{k_h,j}}{\mathrm{i}w}\mathrm{e}^{\mathrm{i}[k_h r-\omega(k_h,j)t]}$ and $\Phi_{k_h,j}=(\mathrm{d}\overline{T}/\mathrm{d}z)W(k_h,j,z)$, Eq. (9) can be reduced to

$$T(z,t)-\overline{T}(z)=\sum_{k_h}\sum_{j}B_{k_h,j}\Phi_{k_h,j}. \tag{10}$$

Substituting Eq. (5) into Eq. (7), it becomes

$$T(z,t)-\overline{T}(z)=\frac{\mathrm{d}\overline{T}}{\mathrm{d}z}\sum_{k_h}\sum_{j}\int a_j(r,t)\mathrm{d}tW(k_h,j,z)\,. \tag{11}$$

When considering $A_j=\int a_j(r,t)\mathrm{d}t$, Eq. (11) can be reduced to

$$T(z,t)-\overline{T}(z)=\sum_{k_h}\sum_{j}A_j\Phi_{k_h j}. \tag{12}$$

Considering the contributions of both the linear and solitary internal waves, the temperature profile can be expressed as

$$\widehat{T}(z,t)=\overline{T}(z)+\sum_{k_h}\sum_{j=1}^{P}(B_{k_h j}+A_j)\Phi_{k_h j}. \tag{13}$$

In other words, the temperature profile can be expanded by the new basis functions $\{\Phi_{k_h j}\}$ (i.e., IWMs), which are derived from the internal-wave eigenmodes. Similar to the EOF method, the first few IWMs often explain much of the temperature information, and the temperature profile can be compressed by retaining only the leading P-order IWMs. The reconstruction mean error (ME) for the temperature test data is

$$\mathrm{ME}=\left|T-\widehat{T}\right|_1/K, \tag{14}$$

where T is the measurement temperature, $\widehat{T}$ is the reconstruction temperature, and K is the total number of the profile's depths. The buoyancy-frequency profile is required to solve the internal-wave eigenmodes. And the buoyancy frequency depends on the background temperature and salinity profile. In other words, the IWM method depends on the background temperature and salinity; if the background field is different, the internal-wave eigenmodes and vertical temperature gradient are different, and thus, the IWMs are distinctive.

The temperature profile can be expanded with both EOFs and IWMs. The EOFs are derived from the temperature data, which represents the mode of data. For adaptability, the temperature samples should cover a complete period of a dynamic ocean activity. The IWMs are derived from the internal-wave eigenmodes, which represent the dynamic ocean modes, and only require the mean (i.e., background) temperature and salinity fields, which can be obtained using fewer measurements. This is validated by an experimental data analysis in Section 4.

4 Experimental results

4.1 *Experimental data*

The experiment was conducted in the South China Sea from September 13, 11:00, to September 17, 06:00, in 2015. A thermistor chain, consisting of 18 temperature–depth sensors (TDs) was used for acquiring the water-column temperature profile over 91 h. The TDs monitored the water column between 13 m and 77 m depth with an approximately 3–4 m depth interval. Considering that the entire temperature profile is required for calculating the new basis functions, isothermal-layer expansion can be utilized for reconstructing the entire temperature profile. The profiles are interpolated to K=201 points, with 0.5 m spacing, and the number of profiles is M=10 921. During the experiment, a conductivity, temperature, and depth (CTD) sensor provided salinity, temperature, and depth measurements near the thermistor chain, from 0.1 m to 100 m depth, with 0.1 m spacing. In this study, we use this salinity data to calculate the buoyancy-frequency profile.

The temperature data are shown in Fig. 1. To evaluate the validity of the two basis functions, the temperatures are divided into two groups. The first 24 h of temperature data (i.e., from September 13, 11:00, to September 14, 11:00, shown in Fig. 1b) are selected for training, and are used for generating the basis functions. The last 67 h of temperature data (i.e., from September 14, 11:00, to September 17, 06:00) are selected for testing. To test the influence of the temperature samples, we generate the basis functions using 1-h, 3-h, 6-h, and 12-h temperature samples. The basis functions are generated by using the temperature data from September 13 at 11:00–12:00, 18:00–19:00, 11:00–14:00, 18:00–21:00, 11:00–17:00, 17:00–23:00, 11:00–23:00, and from September 13, 23:00 to September 14, 11:00, respectively. The background temperature is approximated by taking the average temperature of the corresponding training set. The new basis functions are denoted as IWM11, IWM18, IWM11–14, IWM18–21, IWM11–17, IWM17–23, IWM11–23, and IWM23–11, respectively. The corresponding empirical orthogonal functions are EOF11, EOF18, EOF11–14, EOF18–21, EOF11–17, EOF17–23, EOF11–23, and EOF23–11.

4.2 *Temperature reconstruction*

The first three IWM11 modes are illustrated in Fig. 2 as functions of depth and circular frequency. For this corresponding training set (temperature data from September 13 at 11:00–12:00), the inertial frequency and the maximum value of the buoyancy frequency are 5.2×10^{-5} rad/s and 0.032 rad/s, respectively. Figure 2 shows that the modes are frequency-dependent, and the mode peakedness increases smoothly with frequency.

To analyze the adaptability of the IWM11 at different frequencies, the first five orders of the IWM11 in the frequency from f_c to $N_{\max}$ are used for reconstructing the test set shown in Fig. 1. Figure 3 shows the absolute mean reconstruction error of the 8 041 profiles, which vary at different depths and frequencies. The black dotted line is the mean value over depth, which shows that the mean error increases from 0.25℃ to 0.34℃ with the circular frequency. This shows that the reconstruction accuracy reduces with frequency. The reason is that the internal-wave group speed reduces quickly with frequency. Thus, the higher-frequency modes would have a negligible effect in the far field (Tielbürger et al., 1997). We verify that the same phenomenon is applicable to the other IWM modes. Therefore, in the next sections, we use the IWMs at the lowest frequency (i.e., inertial frequency f_c). The new basis functions are equal to $\Phi_{f_c j}=(\mathrm{d}\widehat{T}/\mathrm{d}z)W(f_c,j,z)$.

Figure 4a shows the buoyancy frequency profile which is generated by using the mean temperature data from September 13 at 11:00–12:00 and the salinity profile measured by CTD. It shows that the buoyancy frequency in the thermocline is large and the maximum is reached to 0.032 rad/s. Figure 4b shows a comparison of the first five IWM11 and EOF11 modes. The solid blue and dotted red lines represent IWM11 and EOF11, respectively. Figure 5 shows the absolute correlation coefficients between the first five EOF11 and IWM11 modes. It is evident that the first five modes of both EOF11 and IWM11 are orthogonal. The first two EOF11 and IWM11 modes are strongly correlated, while the third modes are weakly correlated and the last two modes are almost uncorrelated. The correlation coefficient between EOF_1 and

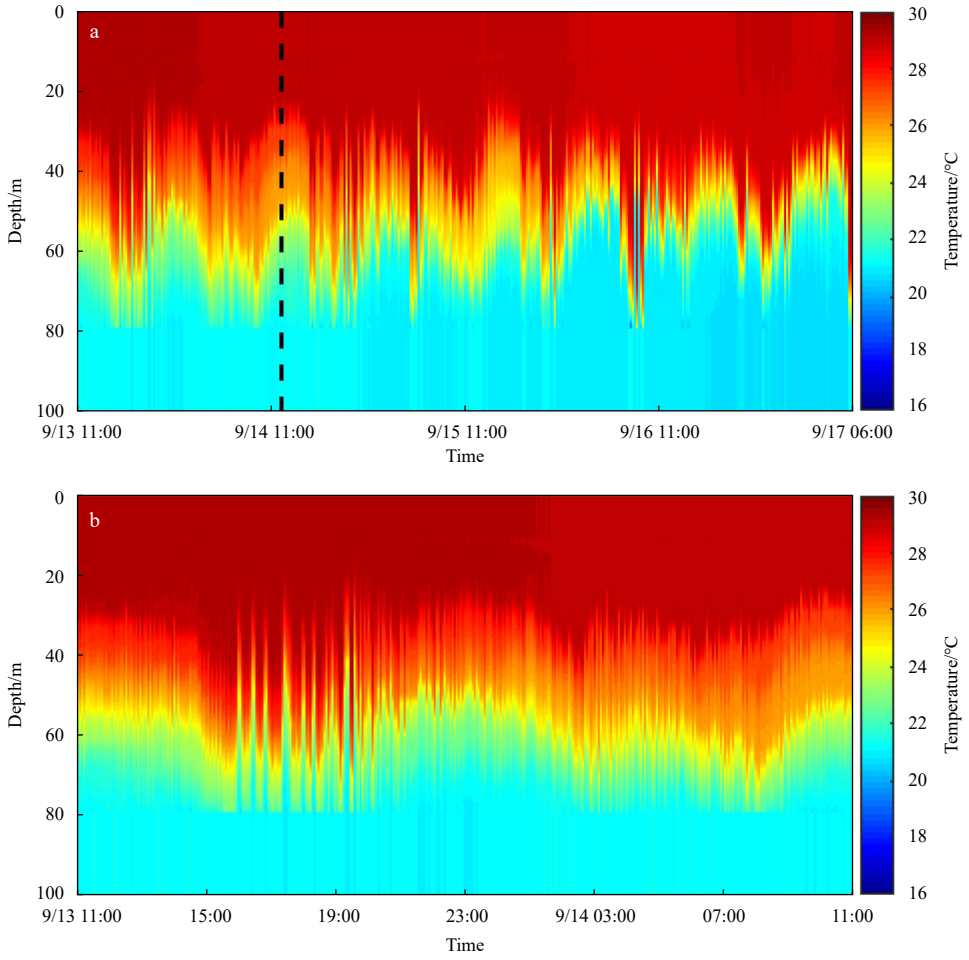

Fig. 1. The experimental temperature data. a. The whole temperature profiles from September 13, 11:00 to September 17, 06:00 (GTM), recorded every 30 s. The data on the left of the black dotted line is the training set, and the data on the right of the black dotted line is the test set. b. The temperature training set.

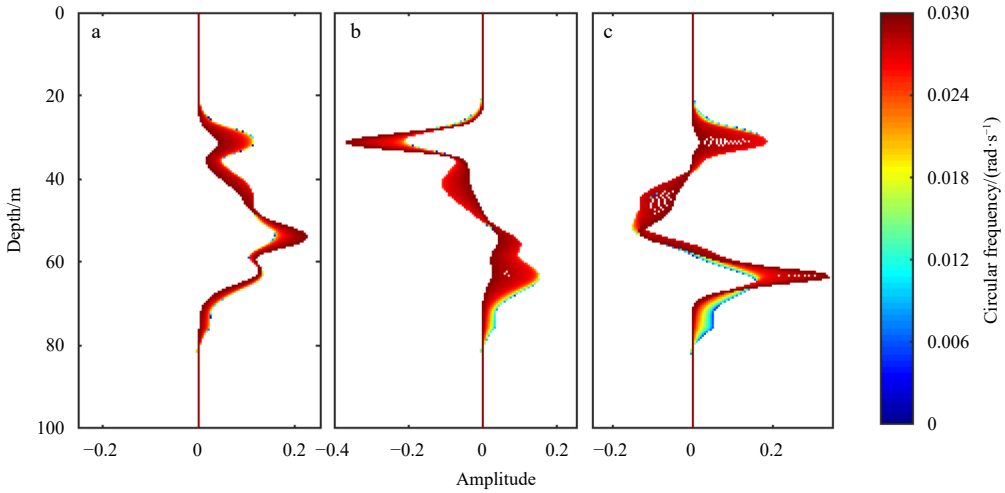

Fig. 2. The first three modes of the IWM11. a. Mode 1; b. Mode 2; c. Mode 3.

IWM_1 is 0.97, and the correlation coefficient between EOF_2 and IWM_2 is –0.92.

We have reconstructed a temperature profile randomly selected in the test set using the first five EOF11 and IWM11 basis functions respectively, and the result is shown in Fig. 6. It is evident that the reconstruction error by IWM11 below 50 m depth is smaller than the EOF11. The reconstruction ME calculated by Eq. (14) is 0.23℃ by the EOF11, and the reconstruction ME is 0.19℃ by the IWM11. So the reconstruction accuracy of the IWM11 is slightly higher.

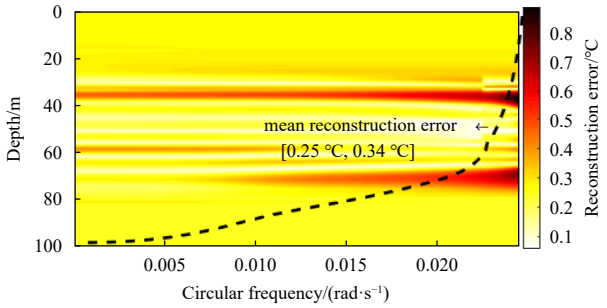

Fig. 3. The mean reconstruction error by the IWM11 in different frequency, together with an overlay of the mean value over depth.

Figure 7 shows a comparison of the first five IWM23-11 and EOF23-11 modes. The solid blue and dotted red lines represent IWM23-11 and EOF23-11, respectively. Figure 8 shows the absolute correlation coefficients between the first five EOF23-11 and IWM23-11 modes. It is evident that the first five modes of both EOF23-11 and IWM23-11 are orthogonal. The first three EOF23-11 and IWM23-11 modes are strongly correlated, and the last two modes are moderately correlated. The correlation coefficient between EOF_1 and IWM_1 is 0.98; the correlation coefficient between EOF_2 and IWM_2 is –0.97; and the correlation coefficient between EOF_3 and IWM_3 is 0.86.

We have reconstructed the same temperature profile as in Fig. 6 with the first five EOF23-11 and IWM23-11 basis functions, and the result is shown in Fig. 9. It is evident that the temperature profile reconstructed by IMW23-11 is in good agreement with the measured profile, and the reconstruction ME is 0.08℃. Although the accuracy of EOF23-11 is improved compared with EOF11, the error at some depths is still large, and the reconstruction ME is 0.17℃.

We have reconstructed the profiles in the test set with the first five modes of the 16 sets of basis functions. Figure 10 shows the mean reconstruction error for each temperature profile, calculated by Eq. (14). The reconstruction error by the EOF method seems to be more unstable, and the IWM method has better reconstruct accuracy than the EOF method in the most situation. For better representation, Fig. 11 shows the average error and the standard deviation of the whole profiles in the test set. The red and blue lines represent the reconstruction errors using the EOF and IWM methods, respectively. It shows that as the sampling length increase from 1 h to 3 h, the reconstruction accuracy of both the IWM and EOF methods is obviously improved. And when the sampling time of the training set is different, the EOF basis function has obvious reconstruction difference, even if the

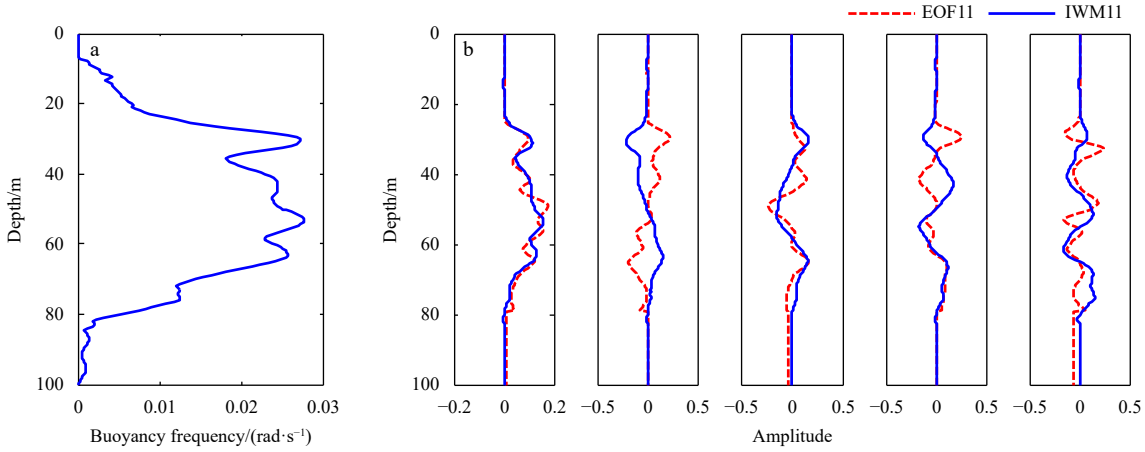

Fig. 4. The buoyancy frequency profile (a) and the comparison of the first five modes of the two basis functions (b). The solid blue line represents the IWM11, and the dotted red line represents the EOF11.

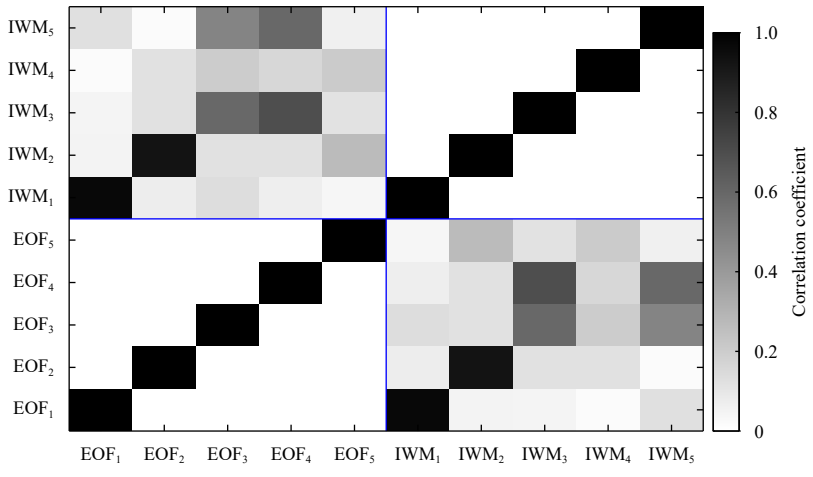

Fig. 5. The absolute correlation coefficients between the first five EOF11 and the IWM11 modes.

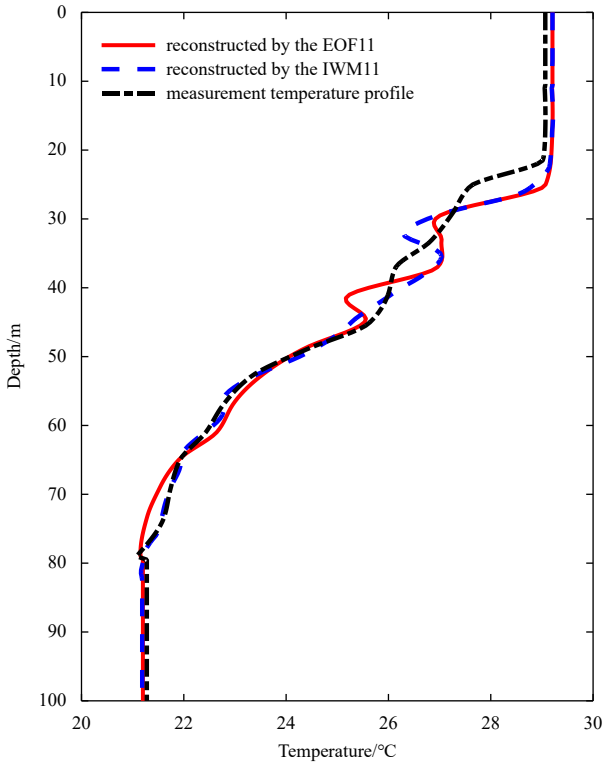

Fig. 6. The reconstruction of a randomly selected temperature profile by five coefficients. The black dotted line represents the measurement temperature profile, the red line represents the reconstruction results by the EOF11, and the blue dotted line represents the reconstruction results by the IWM11.

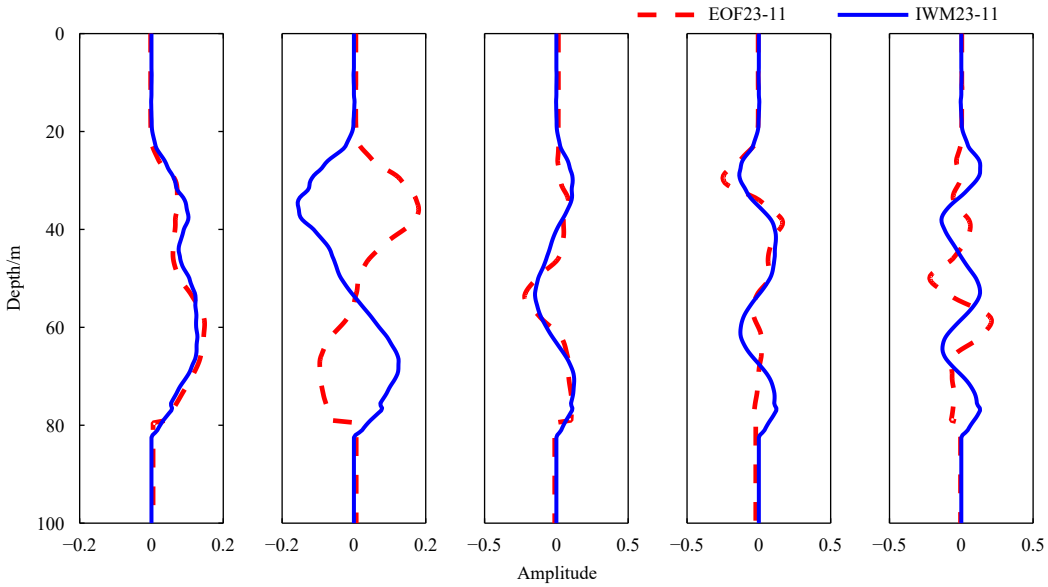

Fig. 7. The comparison of the first five modes of the two basis functions. The solid blue line represents the IWM23-11, and the dotted red line represents the EOF23-11.

sampling length is the same. This shows that the EOF method depends heavily on the sampling time and the sampling length. On the contrary, the IWM method achieved a more accurate reconstruction than that of the EOF method when using the same training set (except for IWM11). In addition, the standard deviation using the IWM method is smaller, which means that the reconstruction accuracy by the IWM method is more stable.

It is also showed in Fig. 11 that the EOF18 has the worst reconstruction accuracy. The reason can be found in Fig. 1 that there are noticeable internal solitary waves from 18:00 to 19:00, so the temperature profiles changes dramatically. This shows that the EOF method is not suitable for the experimental area that is highly variable, and it needs long sample time. Surprisingly, the reconstruction error of the IWM18 is much smaller

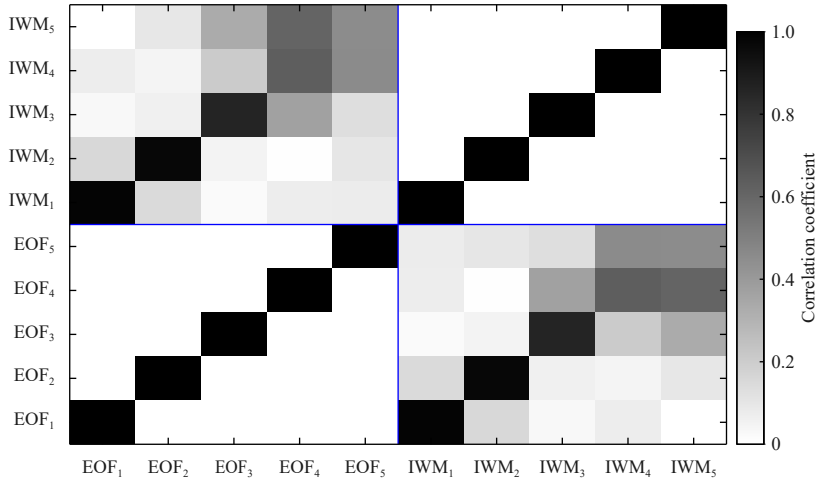

Fig. 8. The absolute correlation coefficient between the first five modes of the EOF23-11 and the IWM23-11.

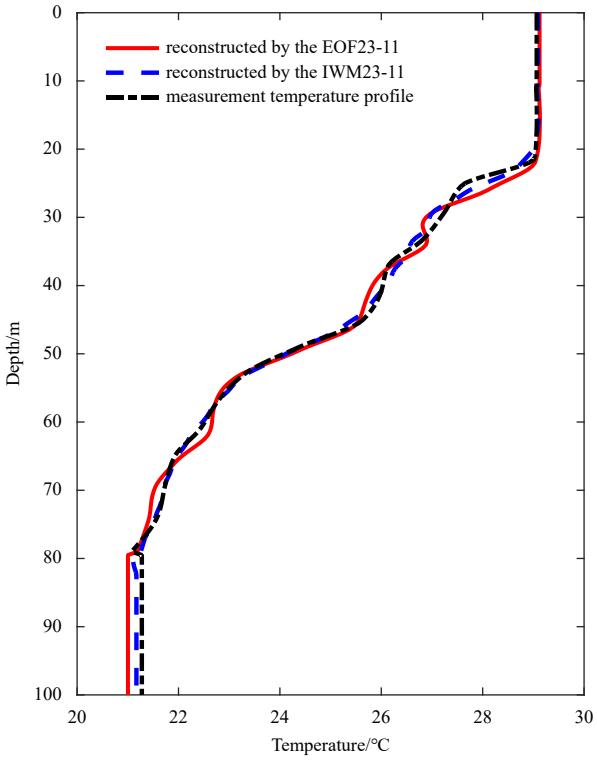

Fig. 9. The reconstruction of the selected temperature profile using five coefficients. The black dotted line represents the measurement temperature profile, the red line represents the reconstruction results using the EOF23-11, and the blue dotted line represents the reconstruction results using the IWM23-11.

than the IWM11. This indicates that the IWM method has a robust reconstruction accuracy for oceanic regions that have internal solitary waves.

In order to test the effective time of the basis functions, Fig. 12 shows the reconstruction error by EOF/IWM11 and EOF/IWM23-11. Since there are many profiles in the test set, for simplicity, the reconstruction error is averaged every 30 min. It shows that as the time distance grows between the test profiles and the training set, the reconstruction error roughly increases. Figure 12a shows that the reconstruction error has large outliers especially for the EOF11. The main reason is that the amount of sample data is insufficient. For example, the EOF11 has a bad applicability for the temperature profiles around September 16, 04:30. And the reconstruction error of other EOF methods is generally large here, which can be seen from Fig. 10. However, the IWM11 could obviously eliminate these outliers. We could find from Fig. 1 that there are internal solitary waves in the ocean region around September 16, 04:30. So we could conclude that the IWM method is more suitable for modeling the temperature fields, especially in the presence of internal waves.

Figure 12a also shows that, after September 16, 04:30, the errors using EOF11 are smaller than those using IWM11. The same

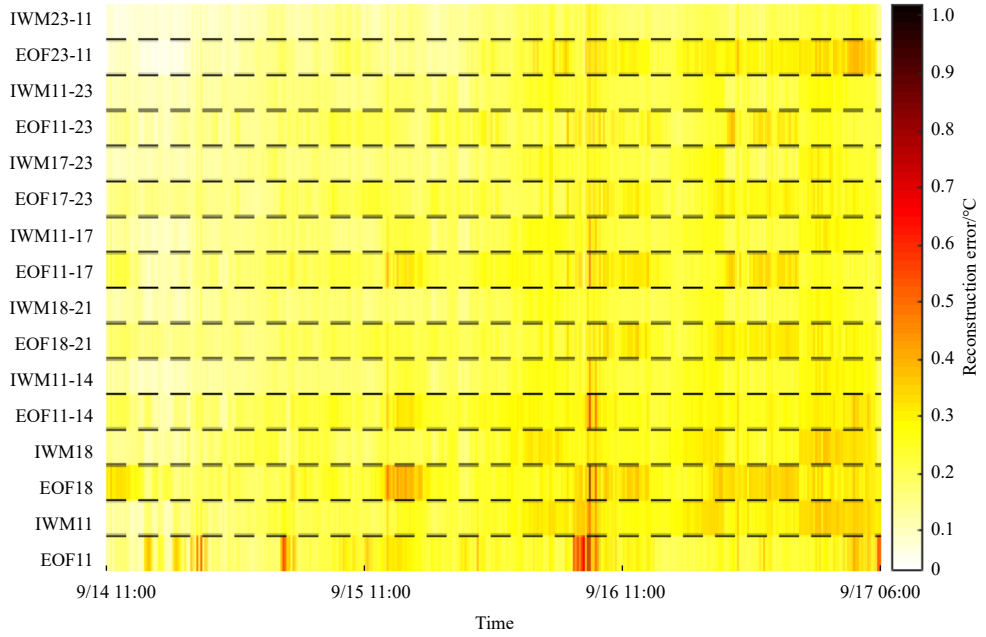

Fig. 10. The reconstruction mean error of the temperature profiles in the test set with the 16 sets of basis functions.

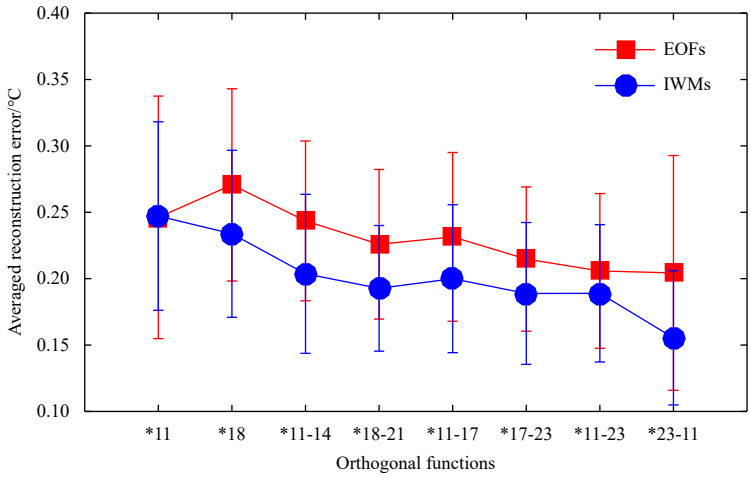

Fig. 11. The average reconstruction errors using the 16 different basis functions. The red square represents the average reconstruction errors using the EOFs, and the blue circular represents the average reconstruction errors using the IWMs. The length of the vertical line represents the standard deviation. * represents EOF or IWM.

phenomenon is also found in the IWM18 and EOF18 shown in Fig. 10. It shows that when the training set is rare, the EOF can be sometimes more accurate than the IWM. The reason is that when the sample time is short, the mean temperature varies greatly from the actual background field. It is certain that the reconstruction error both by the EOF and IWM are large by slight samples (such as 1 h). However, which method is more accurate is random.

5 Summary and conclusions

A new set of basis functions (IWMs) is developed from the internal-wave equation for parameterizing ocean-temperature profiles. The IWMs are generated by combining the internal-wave eigenmodes with the average temperature gradient. The first two basis functions of the EOF and IWM methods are similar, while differences exist mainly in the higher orders. The theoretical analysis and experimental data showed that the IWM method can achieve more accurate reconstructions than those of the EOF method when using the same training samples. The experimental results demonstrate that the IWMs have higher reconstruction accuracy and adaptability in shallow waters even in the situation where internal waves occur frequently. It is worth noting that the internal-wave equation is obtained in shallow water waveguides, and the internal-wave spectrum is different between the deep water and shallow water, so the new set of basis functions are only suitable in shallow water.

The new set of basis functions has higher reconstruction accuracy and adaptability in shallow sea areas such as continental shelf where internal waves occur frequently.

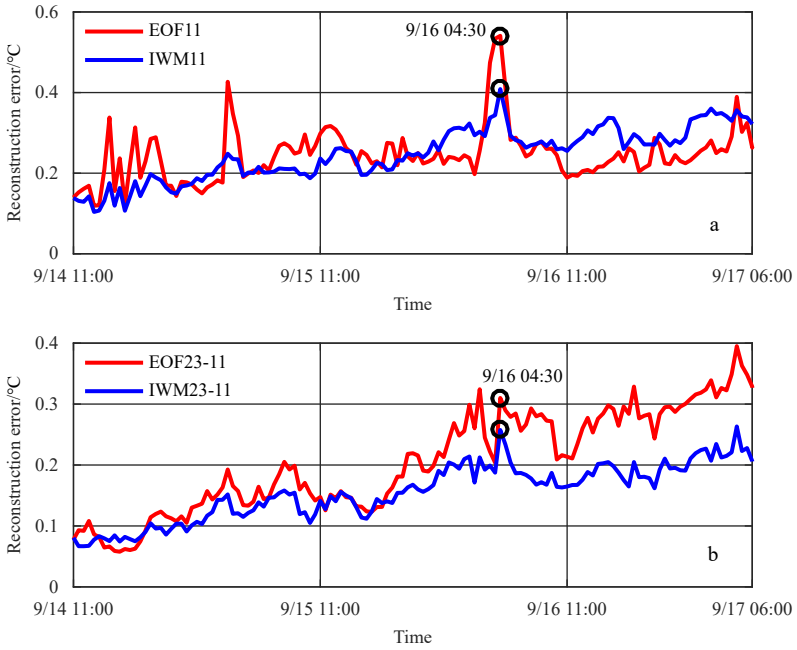

Fig. 12. The average reconstruction errors every 30 min using EOF/IWM11 and EOF/IWM23-11. The red line represents the reconstruction results using the EOFs, and the blue line represents the reconstruction results using the IWMs.

References

Apel J R. 1987. Principles of Ocean Physics. San Diego, CA: Academic Press, 61–121

Jensen F B, Kuperman W A, Porter M B, et al. 2011. Computational Ocean Acoustics. 2nd ed. New York: Springer, 3–10

Kakatkar R, Gnanaseelan C, Chowdary J S. 2020. Asymmetry in the Tropical Indian Ocean subsurface temperature variability. Dynamics of Atmospheres and Oceans, 90: 101142, doi: 10.1016/j.dynatmoce.2020.101142

Li Zhenglin, He Li, Zhang Renhe, et al. 2015. Sound speed profile inversion using a horizontal line array in shallow water. Science China Physics, Mechanics & Astronomy, 58(1): 1–7

Li Qianqian, Shi Juan, Li Zhenglin, et al. 2019a. Acoustic sound speed profile inversion based on orthogonal matching pursuit. Acta Oceanologica Sinica, 38(11): 149–157, doi: 10.1007/s13131-019-1505-4

Li Fenghua, Wang Kai, Yang Xishan, et al. 2021. Passive ocean acoustic thermometry with machine learning. Applied Acoustics, 181: 108167, doi: 10.1016/j.apacoust.2021.108167

Li Fenghua, Yang Xishan, Zhang Yanjun, et al. 2019b. Passive ocean acoustic tomography in shallow water. The Journal of the Acoustical Society of America, 145(5): 2823–2830, doi: 10.1121/1.5099350

Monahan A H, Fyfe J C, Ambaum M H P, et al. 2009. Empirical orthogonal functions: the medium is the message. Journal of Climate, 22(24): 6501–6514, doi: 10.1175/2009JCLI3062.1

Song Wenhua, Hu Tao, Guo Shengming, et al. 2014. A methodology to achieve the basis function for the expansion of sound speed profile. Chinese Journal of Acoustics, 33(3): 299–311

Tan B A, Gerstoft P, Yardim C, et al. 2013. Broadband synthetic aperture geoacoustic inversion. The Journal of the Acoustical Society of America, 134(1): 312–322, doi: 10.1121/1.4807567

Tielbürger D, Finette S, Wolf S. 1997. Acoustic propagation through an internal wave field in a shallow water waveguide. The Journal of the Acoustical Society of America, 101(2): 789–808, doi: 10.1121/1.418039